CELL BIOLOGY

Creating coveted bioluminescence colors for simultaneous multi-color bioimaging

Mitsuru Hattori[1], Tetsuichi Wazawa[1], Mariko Orioka[2], Yuki Hiruta[2], Takeharu Nagai[1,3,4]*

Bioluminescence, an optical marker that does not require excitation by light, allows researchers to simultaneously observe multiple targets, each exhibiting a different color. Notably, the colors of the bioluminescent proteins must sufficiently vary to enable simultaneous detection. Here, we aimed to introduce a method that can be used to expand the color variation by tuning dual-acceptor bioluminescence resonance energy transfer. Using this approach, we could visualize multiple targets with up to 20 colors through single-shot acquisition using a color complementary metal-oxide semiconductor camera. Overall, this method enables simple and simultaneous observation of multiple biological targets and phenomena.

INTRODUCTION

Labeling individual cells within a cell population is important for achieving various research objectives, such as tracking cell fate, observing cell fractionation, and identifying rare cells with distinct characteristics (*1*). Optical markers, such as fluorescence and bioluminescence, are often used to distinguish not only cells in a population but also subcellular structures, cellular proteins, and physiological substances in the same sample. Fluorescent multicolor labeling has been used in a wide range of applications, including the identification of nerve cells (*2*, *3*) and the selection of floating cells by flow cytometry. Although less commonly used than fluorescence, bioluminescence, which is produced by the chemical reaction of luciferin catalyzed by proteins, such as luciferase, eliminates the need for excitation light, avoids autofluorescence, and enables highly sensitive detection with a high signal-to-noise ratio (*4*). A prevalent method for modifying the wavelength of bioluminescence involves the development of specialized bioluminescent substrates. Particularly in in vivo applications, the focus has increasingly shifted toward the creation of long-wavelength light-emitting substrates, which are paired with specific luciferases to enhance biological permeability. This adaptation allows for deeper tissue penetration and reduces light scattering, substantially improving the visibility and utility of bioluminescent signals in live animal studies (*5*–*7*). These developments are crucial for applications that require precise imaging and tracking of biological processes in deep tissues. On the other hand, when individual cells or objects are labeled with bioluminescence and identified in the same space, it is necessary to find differences in the bioluminescence color of the luciferase itself. Multiple luciferase color variants are essential for identifying multiple targets, and species with various bioluminescence colors have been isolated and developed (*5*, *8*, *9*). For imaging applications, such as microscopy, the enhanced Nanolantern (eNL) (*10*), in which the luciferase, NanoLuc (*11*) (Nluc), is fused with a fluorescent protein (FP) to induce bioluminescence resonance energy transfer (BRET), modifies the bioluminescence spectrum to achieve a five-color series. However, these color variants are insufficient for multiple-target observations.

When enough color variants are established, their use in bioimaging becomes the next challenge. In multiplex fluorescence imaging, the observation of more objects reduces the wavelength interval between fluorescent markers, leading to excitation cross-talk. As a result, this situation requires rigorous wavelength control and possibly computational processing, such as spectral unmixing (*12*–*15*). Methods for distinguishing cells and organelles using six to eight different fluorescent molecules have been proposed. These methods comprise a rigorous process that involves separating the excitation and fluorescence wavelengths using a microscope and applying spectral unmixing with a software (*16*–*18*). Although more than 15 fluorescent colors can be separated in biological specimens (*15*), simultaneously observing these colors in the same sample remains limited owing to technical constraints.

The bioluminescence feature of no excitation light eliminates the concerns of excitation cross-talk in multi-labeled specimens. Thus, bioluminescence can further increase the number of colors observed in a sample. However, the relatively broader spectrum of bioluminescence compared with that of fluorescence leads to difficulty in multiplex color imaging. In addition, when multiple markers are applied, the total exposure time increases with an increase in the number of objects, and the individual objects are observed at different times. To overcome this problem, a method was used to simultaneously detect different wavelengths by separating the optical path (*19*–*21*). Yao *et al.* developed a phasor analysis method that is commonly used to distinguish spectrally similar luminophores (*22*). This method enabled easy resolution of the six bioluminescent reporters in live cells via quantitative and instantaneous readouts. However, the detection and distinction of more than 10 bioluminescence colors in biological observations, particularly at the cellular level, have not been reported. To emphasize the importance of observing many objects simultaneously, bioluminescence must abandon the use of switchable optical filters.

To effectively perform multiple-color observations, all wavelengths should be detected simultaneously. Recently, methods to detect bioluminescence comprise color complementary metal-oxide semiconductor (CMOS) cameras, such as smartphone cameras, to capture changes in bioluminescence color (*23*–*25*). Similar to the capture of scenic photos with smartphones, simultaneously

[1]Department of Biomolecular Science and Engineering, SANKEN, Osaka University, 8-1 Mihogaoka, Ibaraki, Osaka 567-0047, Japan. [2]Department of Applied Chemistry, Faculty of Science and Technology, Keio University, 3-14-1 Hiyoshi, Kohoku-ku, Yokohama, Kanagawa 223-8522, Japan. [3]Transdimensional Life Imaging Division, OTRI, Osaka University, 1-1 Yamadaoka, Suita, Osaka 565-0871, Japan. [4]Research Institute for Electronic Science, Hokkaido University, Kita-ku-ku, Sapporo, Hokkaido 001-0020, Japan.
*Corresponding author. Email: ng1@sanken.osaka-u.ac.jp

detecting all wavelengths enables the identification of different bioluminescence colors. Therefore, if the range of bioluminescence colors is sufficiently extensive, simultaneous observation of multiple targets can be realized.

Here, we expanded the color palette by developing a method to modify the bioluminescence color of eNL using another fusion of FP for dual-acceptor BRET. By adjusting the BRET efficiencies between Nluc and the two FPs, we fine-tuned the bioluminescence colors to produce a series of eNL variants with 20 colors. Furthermore, although several color imaging methods generally require multiple consecutive image acquisitions while changing the optical filters, we succeeded in obtaining a time-lag–free single-shot observation of many colored cells using a color CMOS camera.

RESULTS

Expanding the bioluminescence color hue by dual-acceptor BRET

Currently available eNLs have five color variants: CeNL (cyan), GeNL (green), YeNL (yellow), OeNL (orange), and ReNL (red) (*10*). To further increase the eNL color variants, we hypothesized that additional fusion with an FP could enhance the spectrum. Such fusion may induce another BRET that leads to a color change, not only via an increase or decrease in the original luminescence peak intensity but also via the generation of another peak (Fig. 1A). To demonstrate its feasibility, we fused enhanced green fluorescent protein (eGFP) to the C terminus of CeNL (Fig. 1B, CeNL-eGFP). The change in the emission color of CeNL-eGFP was confirmed via a comparison with the original CeNL, GeNL, and Nluc. Upon combination with its substrate, coelenterazine-h (CTZh), the bioluminescence color of CeNL-eGFP differed from that of the original based on image capture using a smartphone CMOS camera (Fig. 1C). The bioluminescence spectrum of CeNL-eGFP had an additional peak compared to that of CeNL (wavelength, 512 nm), with a decrease in the original peak (wavelength, 474 nm) (Fig. 1D). Of note, such complex spectrum is difficult to obtain by simply replacing the FP of the eNL with another. Dual-acceptor BRET might increase spectral variation in eNL.

On the basis of the dual-acceptor BRET concept, we designed eNL variants in which different types of FPs were fused to the C terminus of the eNLs (fig. S1). In addition, three eNL variants were developed based on the mCherry variants (mCXL2NL, mCXL7NL, and mCRedNL; Supplementary Materials). When expressed in *E. coli* colonies, these genes produced bioluminescence colors that were detectable by a smartphone camera (Fig. 2A). The purified protein from the *E. coli* showed 20 distinct colors (Fig. 2B), which is the largest color variation observed for bioluminescent proteins using the same luminescent substrate. The expanded color palette of the bioluminescent proteins was denoted as eNLEX (eNL expansion). Notably, the number of colors can be further increased by changing the combination of FPs. As demonstrated by images captured with a smartphone camera, eNLEX serves as a bioluminescent marker for many targets that can be simultaneously and easily distinguished without changing the optical filters.

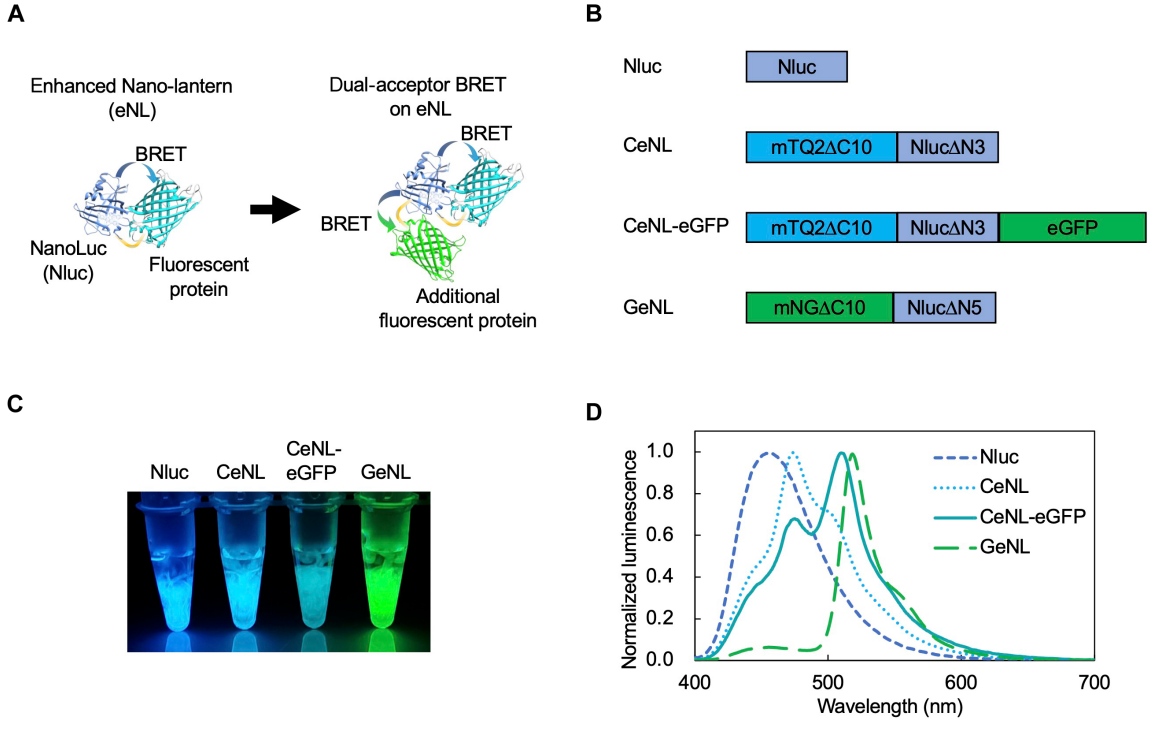

Fig. 1. Spectrum changes in eNL by the introduction of dual-acceptor BRET. (**A**) Schematic representation of the spectrum changes in enhanced Nano-lantern (eNL) with the dual acceptor. (**B**) Protein structures of the luciferases. mTQ2, mTurquoise2; mNG, mNeonGreen. eGFP was fused to the C terminus of CeNL. (**C**) Bioluminescence images of purified Nluc and eNL variants captured using a smartphone camera. Substrates were added to the purified proteins. Exposure time: 0.5 s. (**D**) Bioluminescence spectra of the eNL variants. Intensities were normalized to their respective peak values.

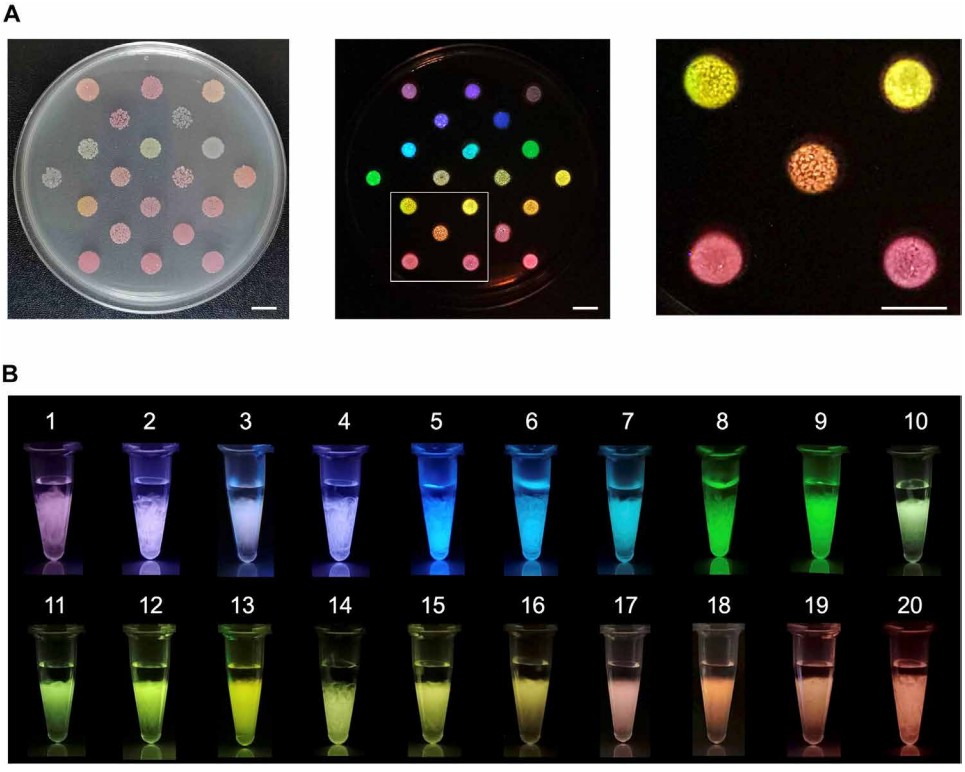

Fig. 2. Twenty-color variants of bioluminescent proteins, eNLEX. (**A**) *E. coli* colonies expressing each bioluminescent protein. Brightfield image (left), bioluminescence image (middle), and the enlarged image of the white square (right) are shown. Exposure time for bioluminescence: 10 s. Scale bar, 10 mm. (**B**) Bioluminescence images of purified eNLEX members captured using a smartphone camera. 1: mCRedNL-tdT, 2: mCXL7NL, 3: CeNL-tdT, 4: mCXL2NL, 5: Nluc, 6: CeNL, 7: CeNL-eGFP, 8: GeNL, 9: YeNL, 10: OeNL-mTQ2, 11: OeNL-eGFP, 12: OeNL-Venus, 13: GeNL-tdT, 14: OeNL, 15: OeNL-mKOκ, 16: OeNL-tdT, 17: ReNL-eGFP, 18: ReNL-Venus, 19: ReNL-mKOκ, 20: ReNL. Exposure time: 0.5 s.

Slight color change of eNLEX based on adjustment of the intermolecular distance

The color variation of eNLEX was mainly due to a combination of multiple spectral peak wavelengths and differences in their peak ratios (fig. S2). As the intensity of each peak relies on the corresponding BRET efficiency and fluorescence quantum yield, adjusting the distance between Nluc and the FPs enables fine-tuning of subtle color differences. Using OeNL-mTurquoise2 (mTQ2) and OeNL-eGFP, we examined whether the color could be adjusted. OeNL and FP were connected via a Glu-Phe (EF) linker. To maintain a constant distance, other constructs were prepared using the rigid linker, Glu-Ala-Ala-Ala-Lys (EAAAK) (Fig. 3A). The linkers were observed to affect the bioluminescence color (Fig. 3B). For OeNL-mTQ2, the peak from mTurquoise2 (approximately 475 nm) decreased with a rigid linker (OeNL-r-mTQ2) (Fig. 3C). OeNL-eGFP exhibited three peaks derived from Nluc, eGFP, and mKOκ (Fig. 3D). Introduction of the rigid linker (OeNL-r-eGFP) induced a decrease in the eGFP peak (approximately 525 nm) and an increase in the Nluc peak (approximately 460 nm) (Fig. 3D). When the original eNLs were developed, five different colors were obtained by examining the number of deletions at each terminal of the protein and the type of amino acid used as the linker (*10*). This method can be used to generate a wide range of bioluminescence colors, including minor differences, through adjustments of the length of the linker attached to the additional FP.

Simultaneous multiple-color imaging of bioluminescent cells with a color CMOS camera

eNLEX can be used as a marker for multiple targets. As bioluminescence requires no excitation light, we can simultaneously detect and identify multiple wavelengths as distinct colors, as depicted in the image in Fig. 2A, which was obtained with a smartphone camera. However, owing to the insufficient intensity of bioluminescence or the limited use of highly sensitive color cameras, current microscopy methods for observing multiple bioluminescence markers typically rely on a combination of cooled electron-multiplying charge-coupled device (EMCCD) cameras and band-pass filters for sequential detection. We attempted to capture bioluminescent images of living cells using a color CMOS camera. HeLa cells expressing each of the 20 color variants of the eNLEX were prepared, and their bioluminescence was observed using a camera attached to a conventional microscope. Cells emitting 20 different bioluminescence colors were detected, despite the requirement of tens of seconds of exposure to the camera (Fig. 4A). The differences in the bioluminescence colors among the cells could be distinguished even when mixed and cultured (Fig. 4B). Even in different cultured cell types and plant cells, the bioluminescence color can also be distinguished (fig. S3). The performance of bioluminescence imaging using color cameras is not limited to the eNLEX. D-Luciferin–based luciferases, such as firefly luciferase, can be captured using a color camera under certain conditions. Thus, we simultaneously captured luminescence from cells expressing Eluc (*26*) and Akaluc (*6*) (fig. S4). On the basis of our

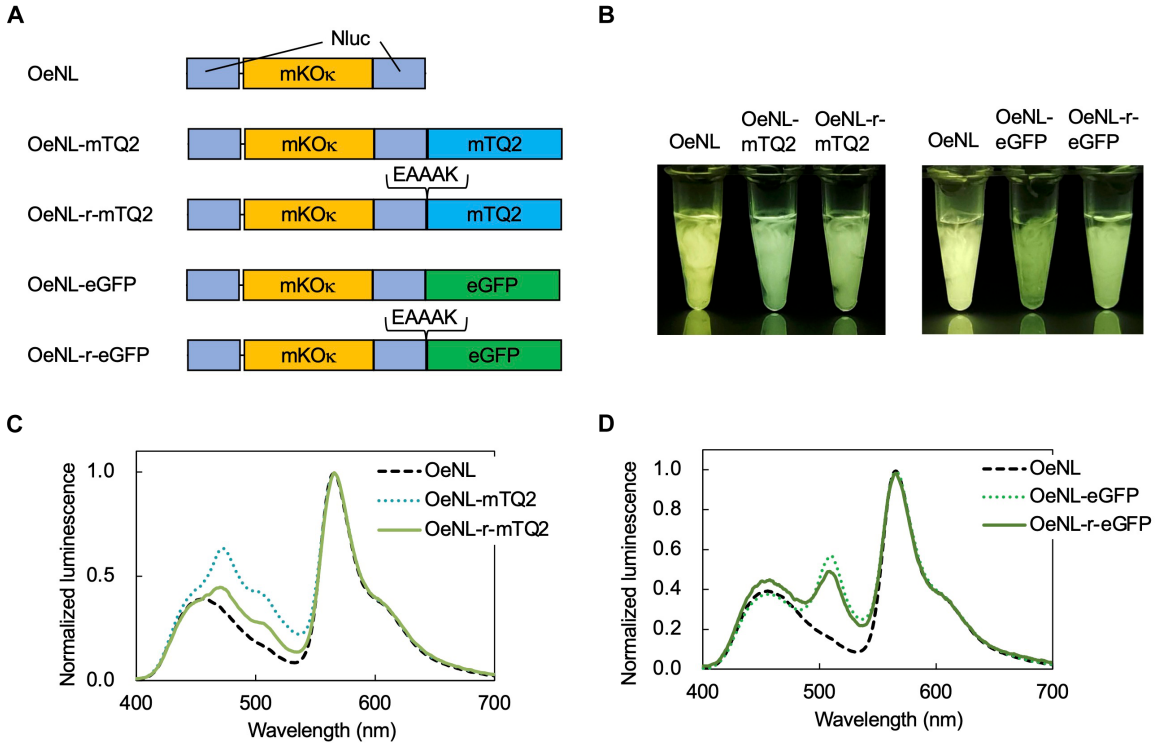

Fig. 3. Adjusting bioluminescence colors by inserting linkers. (**A**) Protein construction of OeNL, OeNL-mTQ2, OeNL-rigid(r)-mTQ2, OeNL-eGFP, and OeNL-r-eGFP. The sequence of the rigid linker is also shown. (**B**) Bioluminescence images captured using a smartphone camera. Exposure time: 0.5 s. (**C**) Bioluminescent spectra of OeNL, OeNL-mTQ2, and OeNL-r-mTQ2. The intensities were normalized to the peak intensity. (**D**) Bioluminescent spectra of OeNL, OeNL-eGFP, and OeNL-r-eGFP.

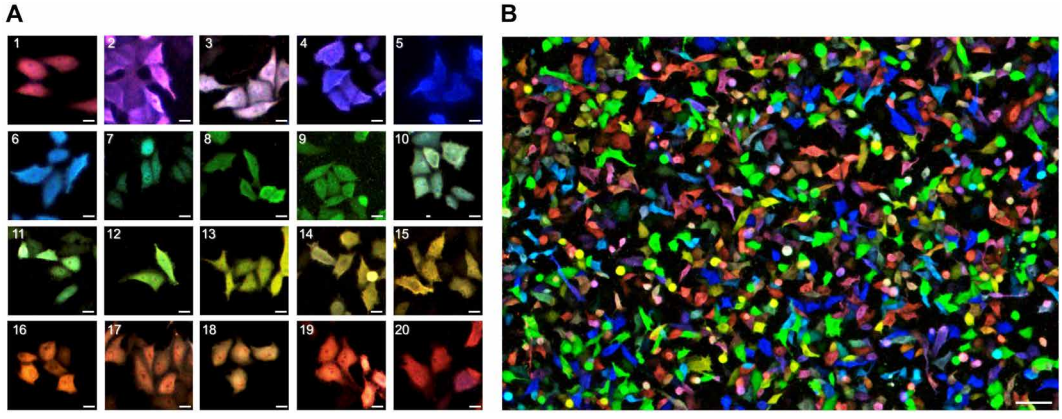

Fig. 4. Expression of eNLEX in HeLa cells. (**A**) Bioluminescence images of HeLa cells expressing each of the eNLEX members. The images were captured using a color CMOS camera. 1: mCRedNL-tdT, 2: mCXL7NL, 3: CeNL-tdT, 4: mCXL2NL, 5: Nluc, 6: CeNL, 7: CeNL-eGFP, 8: GeNL, 9: YeNL, 10: OeNL-mTQ2, 11: OeNL-eGFP, 12: OeNL-Venus, 13: GeNL-tdT, 14: OeNL, 15: OeNL-mKOκ, 16: OeNL-tdT, 17: ReNL-eGFP, 18: ReNL-Venus, 19: ReNL- mKOκ, 20: ReNL. Exposure time: 15 to 30 s. Scale bar, 20 μm. (**B**) Simultaneous multiple-color bioluminescence imaging of a cell mixture expressing each of the eNLEX members. Exposure time: 30 s. Scale bar, 100 μm.

results, a color CMOS camera can detect multiple bioluminescence colors in a single shot, enabling enormous multiplex color imaging without a time lag.

Application of eNLEX to bioimaging

Simultaneous multi-color bioluminescence imaging with the eNLEX can be used to detect various biological specimens. We constructed cell spheroids to demonstrate the ability of eNLEX to detect individual cells within complex cellular structures. HeLa cells transiently expressing each of the seven color variants of eNLEX were cultured to generate spheroids. Each cell within the spheroid was observed to have a distinct bioluminescence color (Fig. 5A). Furthermore, we applied simultaneous bioluminescence imaging for cell identification and observation across various spatial scales, from complex cell structures to subcellular levels. To confirm our results, we attempted simultaneous multi-color observation of subcellular structures. Each eNLEX member was fused with a localization signal and expressed in cells. As shown in Fig. 5B and fig. S5,

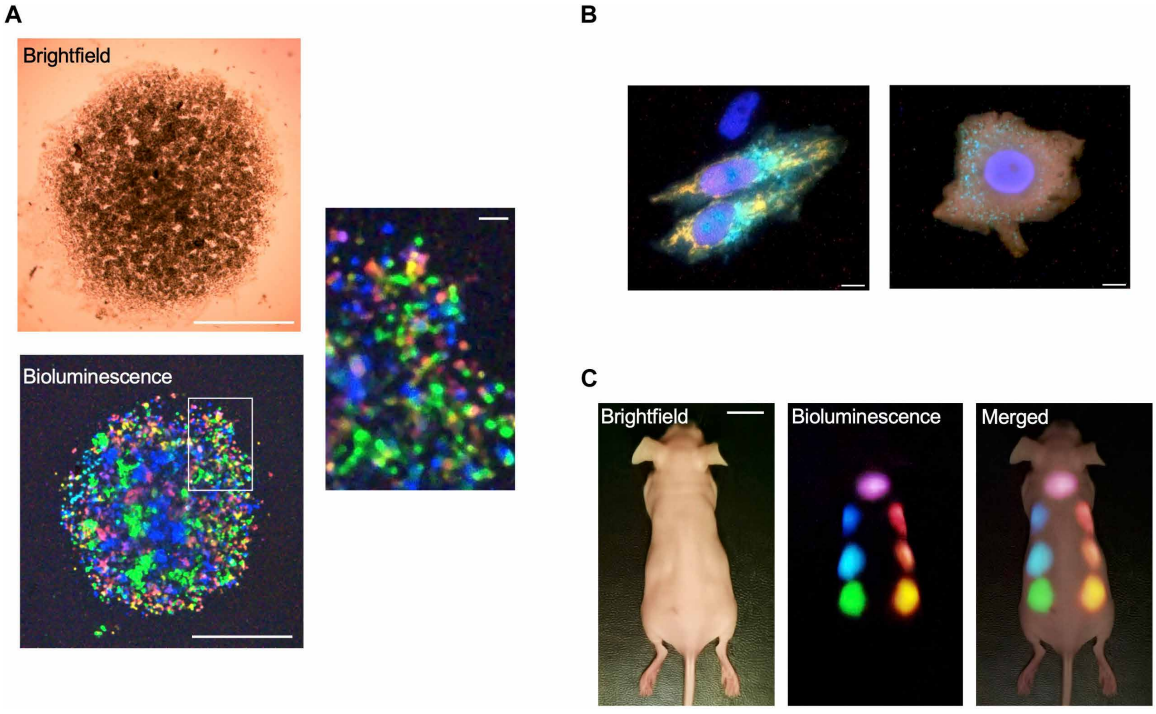

Fig. 5. Multi-scale application of eNLEX. (**A**) Brightfield (upper left) and bioluminescence imaging (lower left and right) of cell spheroid. HeLa cells expressing seven eNLEX members (mCXL7NL, Nluc, CeNL-eGFP, GeNL, GeNL-tdT, OeNL-tdT, and ReNL) were cultured in the same well and observed. Exposure time: 30 s. Scale bar, 1 mm. The enlarged image of the white square in the lower left panel is also shown in the right panel (scale bar, 100 μm). (**B**) Bioluminescence imaging of HeLa cells using eNLEX targeted to subcellular components. Left: GeNL-tdT targeted to the mitochondria, mCXL7NL to the nucleus, CeNL to the lysosome, Nluc to the nucleolus. Right: OeNL-tdT was localized to the cell membrane, while mCXL7NL targeted to the nucleus, CeNL to the peroxisome, and ReNL to the nucleolus. Exposure time: 30 s. Scale bar, 10 μm. (**C**) Simultaneous detection of multiple bioluminescence in a mouse. Images of a mouse transfected with HEK293 cells expressing seven (mCXL7NL, Nluc, CeNL, GeNL, GeNL-tdT, OeNL-tdT, and ReNL) colors of eNLEX captured using a smartphone camera. Exposure time: 10 s. Scale bar, 10 mm.

the organelles [nucleus, nucleolus, cell membrane, mitochondria, lysosome, peroxisome, and endoplasmic reticulum (ER)] were successfully visualized using different colors. The lateral spatial resolution of images provided by the color CMOS camera was sufficiently high to enable detailed observation of mitochondrial fission and fusion (fig. S6). These intracellular expressions of eNLEX indicate that there is no notable disturbance to normal cellular activity or structure (fig. S7). At the individual animal level, bioluminescence imaging is often used instead of fluorescence imaging. However, only few reports describe the multi-color observation of bioluminescence in individual animals. To verify the observability of each eNLEX color, we subcutaneously introduced cells expressing each of the seven color variants of the eNLEX into mice. As shown in Fig. 5C and fig. S8, we confirmed the simultaneous capture of bioluminescence signals from each eNLEX member. Thus, simultaneous bioluminescence imaging is highly applicable over a wide range of spatial scales.

Tracking the behavior of living cells through simultaneous multi-color bioluminescence imaging

When bioluminescence imaging is performed using a color CMOS camera, information regarding emission wavelengths is recorded using red, green, and blue (RGB) filters on the sensor chip. This information allows the separation of each eNLEX bioluminescence color after image capture. To achieve this objective through time-course observations, human embryonic kidney (HEK) 293 cells expressing each of the seven color variants of eNLEX were monitored for several hours. Although furimazine is an optimal luminescent substrate for Nluc (*11*), its bioluminescence cannot be stably maintained over a long period owing to catalytic oxidation in the medium (*27*). As a result, caged furimazines have been developed (*27*–*30*). Our experiments demonstrated that the bioluminescent color emitted by eNLEX is consistent across different substrates, showing no observable variations among the cell types tested (fig. S9). Here, we selected Piv-FMZ (*27*) for our observations, considering the balance between the intensity and stability of bioluminescence. Using this substrate, we tracked the behavior of the cells of each color for approximately 6 hours (Fig. 6, A and B, and movie S1). By converting the RGB information of the captured images into the hue, saturation, and value (HSV) format (*31*), cells were distinguished by their bioluminescence color (Fig. 6C, movie S2, and fig. S10A). Using a similar process, cells of each color in the cell spheroid image could also be distinguished (fig. S11). For longer-time imaging, we also utilized another substrate, endurazine (*28*), which enabled continuous monitoring of cell migration and differentiation with each color over longer periods without detectable degradation in signal intensity (movie S3).

The distinction of each bioluminescence color can be applied to monitor not only the difference between cells but also the change in the bioluminescence spectrum. Several bioluminescence indicators have been developed to detect biological targets by changing their emission color (*19*, *20*, *32*–*34*). To demonstrate the effectiveness of simultaneous multi-color bioluminescence imaging, intracellular

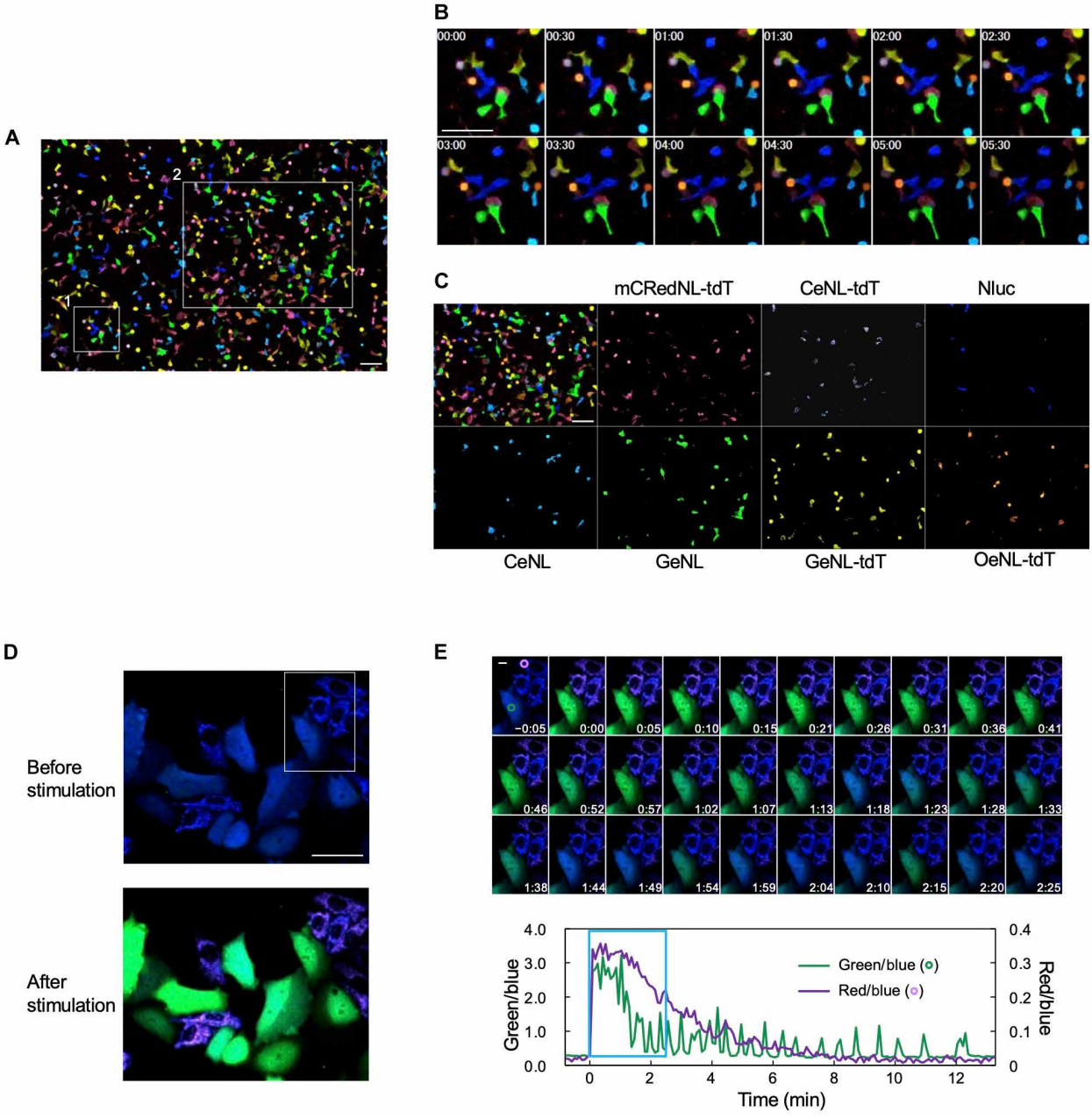

Fig. 6. Time-lapse observation of cells via simultaneous multi-color bioluminescence detection. (**A**) Simultaneous multi-color observation of HEK293 cells with bioluminescence. The movie is available as movie S1. Each of the seven eNLEX members (mCRedNL-tdT, CeNL-tdT, Nluc, CeNL, GeNL, GeNL-tdT, and OeNL-tdT) was expressed in cells and cultured as a mixture. Exposure time: 1 min for each image. Scale bar, 100 μm. (**B**) Time-course observation of cells by multiple bioluminescence color in region 1 shown in (A). Time on images indicate the elapsed time (hours:minutes). Scale bar, 100 μm. (**C**) Separation of the cell image by each bioluminescence color in region 2 shown in (A). The emission color of each luciferase was distinguished by the RGB information. (**D**) Bioluminescence imaging of intracellular Ca^{2+} changes. HeLa cells expressing bioluminescent Ca^{2+} sensors, ORCA-Y (cytosol) and ORCA-R (mitochondria), were observed using a color camera. Cells were stimulated by the addition of histamine. The white square indicates the image area in (D). Exposure time: 5 s. Scale bar, 50 μm. (**E**) Time course of Ca^{2+} based on bioluminescence detection. The time displayed on the images indicates the elapsed time after the addition of histamine in minutes and seconds. The graph shows the luminescence changes in hue in the green and purple circle regions on the image. The blue square indicates the range of images shown. Scale bar, 10 μm.

Ca^{2+} changes were tracked using the ratiometric Ca^{2+} bioluminescence sensors, ORCA-Y and ORCA-R (*35*). In the presence of Ca^{2+}, the respective bioluminescence colors changed from blue to green (ORCA-Y) and blue to purple (ORCA-R). As these bioluminescence color changes are based on BRET, they serve as good examples for testing the application of eNLEX to indicators. The sensors were found to localize in the cytosol and mitochondria. In particular, upon the addition of histamine, the bioluminescence colors in the cytosol and mitochondria changed from blue to green and blue to purple, respectively (Fig. 6D and movie S4). These color changes indicate transient increases and decreases in mitochondrial Ca^{2+} and cytosolic Ca^{2+} oscillations, respectively (Fig. 6E).

To demonstrate the ability to distinguish individual phenomena by their bioluminescent colors, we detected the activity of G protein–coupled receptor (GPCR). By introducing LgBiT-SmBiT (*13*), a complementation system of Nluc, into eNLEX, bioluminescence is generated when the two components interact. This system was combined with the interaction of GPCR and β-Arrestin2, allowing individual activities to be distinguished by their respective bioluminescence colors (Fig. 7A). Each GPCR was fused to the N-terminal part of different eNLEX members: GeNL, CeNL, and mCXL7NL. Each emission was detected by its color upon the addition of a specific ligand (Fig. 7B). Furthermore, by mixing cells expressing different GPCR, multiple GPCR activities could be tracked simultaneously (Fig. 7C). Time-lapse bioluminescence observation revealed that not only do different GPCR species exhibit distinct patterns but also cells of the same species show variation (fig. S12 and movie S5). Similar to the principle of wavelength variation in eNLEX, additional FPs allowed the detection of GPCR activity with different emission colors, which can be distinguished in cell observations (fig. S13).

DISCUSSION

By conducting a dual-acceptor BRET, we successfully developed an eNLEX with 20 bioluminescence colors and demonstrated its application for cell identification. Altogether, eNLEX can be used to simultaneously image all 20 colors with a color CMOS camera, indicating the potential of extending this observation technique to widely available color cameras, including smartphones.

Bioluminescence, which does not require excitation light, is a potential alternative to circumvent the limitations of fluorescence imaging. However, several issues, notably the limited variety of available colors, have prevented its widespread use. Different methods can be used to change the bioluminescence spectrum of luciferase, such as the introduction of mutations in luciferase to change contact with substrates (*5*, *6*, *36*) and the development of substrates (*37*, *38*). Using BRET combined with fluorescent molecules allows the prediction of spectral changes and the high-probability creation of variants (*10*, *39*–*43*). However, this method is limited due to the design and expansion of bioluminescence colors. Our method employs dual-acceptor BRET from Nluc using two FPs. This principle increased the variety of FPs used as acceptors and markedly

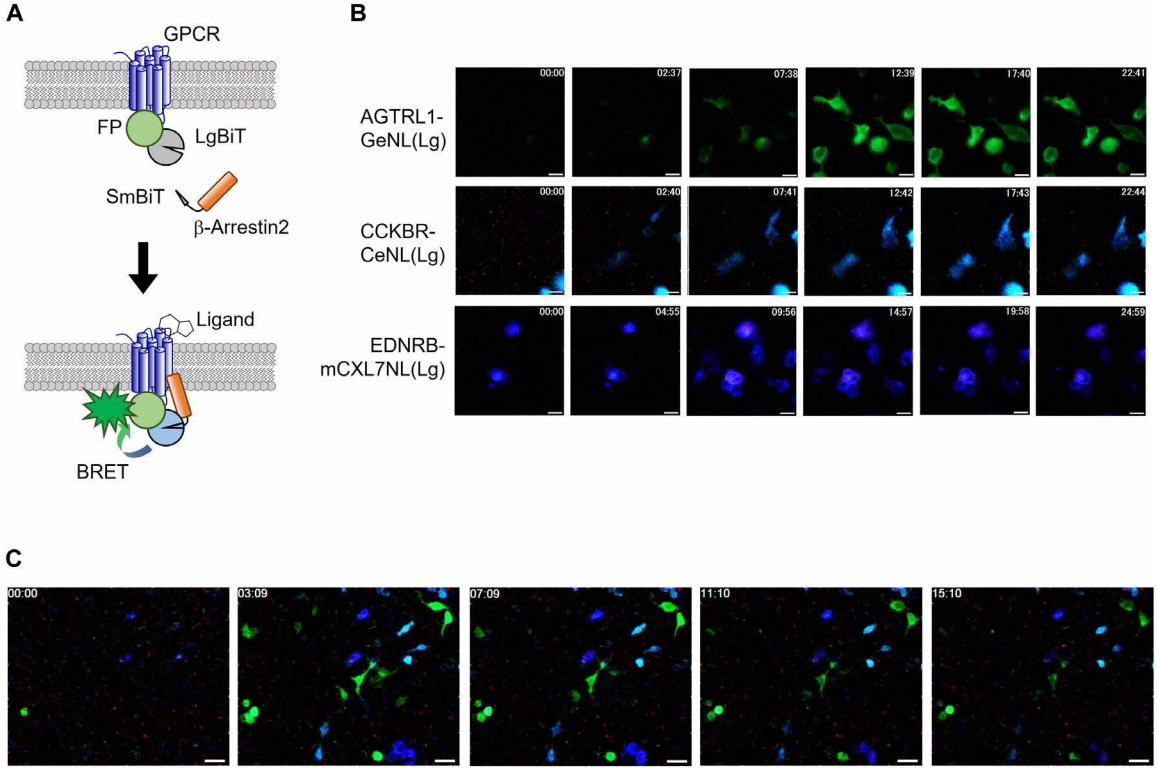

Fig. 7. Observation of multiple GPCR activities in living cells by eNLEX. (**A**) Schematic illustration of the detection system. (**B**) Time-course observation of HEK293 cells expressing individual GPCR activity sensors. The GPCR and eNLEX used for each sensor were shown on the left. The cells were treated with 1.0×10^7 M aperin-13 to AGTRL1, 1.0×10^7 M gastrin-1 to CCKBR, and 1.0×10^6 M endothelin-1 to EDNRB between the first and second images. Exposure time: 2 min for each image. Scale bar, 20 μm. The time displayed on the images indicates the elapsed time in minutes and seconds. (**C**) Simultaneous multi-color observation of GPCR activity by bioluminescence. Each ligand was added simultaneously to cells expressing each GPCR sensor in (B). Exposure time: 2 min for each. Scale bar, 50 μm.

expanded the number of colors that could be represented by bioluminescence. The relative intensities of multiple peaks must be controlled to express slight color differences. Here, we showed that such control can be achieved by simply changing the length or type of linkers that connect FP to Nluc. The original eNLs were developed by combining terminally truncated proteins to achieve maximum BRET (*10*). Modifying these parts is also effective for further increasing the variety of bioluminescence colors. In addition to the existing eNL, we developed a "purple" eNL using a combination of red FPs and Nluc. Further trials involving long Stokes-shifted FPs can efficiently shift the Nluc luminescence to longer wavelengths. Because of the properties of Nluc and the fused FPs, some of eNLEX members are influenced by environmental conditions. The spectra of members with multiple peaks vary depending on pH and temperature (figs. S14 and S15). It is preferable to select an eNLEX member with a single peak under large environmental changes or when a stable wavelength is required.

The low luminescence intensity, another weakness of bioluminescence compared to fluorescence, has almost been completely overcome by Nluc and its derivatives for application in microscopic imaging (*10*, *11*). Bioluminescence imaging now offers subsecond temporal resolution. However, when multi-color imaging is performed, the emission filters must be switched to acquire each image. Therefore, multi-color imaging using the eNLEX, which has up to 20 colors, is extremely time consuming. To overcome this limitation, we used a color CMOS camera and captured images of cells expressing 20 of the eNLEX colors through single-shot imaging.

The absence of external excitation light makes bioluminescence particularly useful for detecting signals from deep within the animal body. On the other hand, light penetration varies with wavelength, affecting the bioluminescence color. The color CMOS camera could also detect the bioluminescence of eNLEX deep within a mouse, although eNLEX with multiple wavelength peaks changed from their natural colors (fig. S16). Currently, it is not envisioned that we will perform multi-color simultaneous imaging deep within the living body. This method can be used to analyze drug responses with subcutaneously expressed sensors.

By converting the format of the acquired images from RGB to HSV, we successfully identified cells with different bioluminescence colors. As this difference can be seen and recognized, an RGB representation of a bioluminescent image is sufficient for the human eye to identify colors. However, for automated identification, quantifying more subtle differences through the hue and saturation indices in the HSV format is effective. The combination of bioluminescence and a color CMOS camera takes a similar approach to human vision, detecting all colors simultaneously in the RGB format and later distinguishing them via information processing. Currently, it is challenging to perfectly identify eNLEX members that are similar in hue or close in cell (figs. S10A and S17). Therefore, the method is useful primarily for identifying cells in a population. The activities of different GPCR species between cells could be detected simultaneously and analyzed separately (fig. S12). There were differences in the time course of the same GPCR species, which could be classified into three trends. It has been shown that the time course of GPCR activity is characteristic for each GPCR species (*44*, *45*). This is the first analysis to clarify differences between cells by measuring multiple types simultaneously.

With the widespread use of smartphones, CMOS image sensors have become mainstream in camera development (*46*). The use of monochrome CMOS cameras has become common for fluorescence methods used in scientific research. However, bioluminescence has not had a similar adoption. In our study, the simultaneous observation of multi-color bioluminescence was demonstrated by combining a color CMOS camera and eNLEX. The observation equipment is simpler because a switching optical filter is not required, thereby reducing cost. Although the cameras used in this study were not optimal for bioluminescence imaging, their detection sensitivity was capable of capturing bioluminescence (figs. S18 and S19). The exposure time or the gain can be adjusted according to the bioluminescence intensity of the object. A more suitable color camera will be developed for future bioluminescence imaging. By improving its sensitivity and reducing the intrinsic noise, the exposure time for bioluminescence can be further shortened, potentially enabling more rapid observation. The linearity and gamma correction of RGB cameras should also be considered in quantitative measurements. The combination of EMCCD and eNLEX effectively enhances sensitivity and resolution in imaging. By efficiently using optical filters, EMCCD detection expands the possibilities of multicolor bioluminescence imaging.

For satisfactory bioluminescence observations, a substrate and a camera must be selected. As demonstrated here, the use of caged substrates is effective at enabling stable observation as the oxidation caused by medium components is suppressed. If the purpose is limited to tracking rapid changes, the selection of a high-intensity substrate, such as the original furimazine, enables observations with a shorter exposure time. Thus, a desired image can be acquired using a suitable combination of camera and substrate.

Multi-color bioluminescence imaging has additional advantages over fluorescence imaging. One of the advantages of bioluminescence, which does not require excitation light, lies not only in the identification of targets but also in the absence of phototoxicity to the cells under observation. In optogenetics, which has gained popularity in recent years, light stimulation and bioluminescence work well when used within the same field of view (*47*, *48*). For substrate addition, which has also been a bottleneck for bioluminescence observations, the introduction of an auto-luminescence system, including substrate synthesis (*49*, *50*), into a target species is expected to be convenient. By integrating the eNLEX technology into these bioluminescence systems, it is possible to achieve multicolor detection without the addition of substrate. By using the method to create color variations and simultaneously observe multiple targets, the versatility of bioluminescence imaging can be further expanded.

MATERIALS AND METHODS

Plasmid DNA

For the purification of proteins from *E. coli*, plasmids expressing Nluc and eNL proteins (CeNL, GeNL, YeNL, OeNL, and ReNL) were used as described elsewhere (*6*). For fusion with FP at the C terminus, cDNAs of stop codon–deleted eNL were amplified using polymerase chain reaction (PCR). The DNA oligonucleotides used for PCR were purchased from Hokkaido System Science. KOD-plus Neo (Toyobo Life Science) was used for PCR amplification. The amplified products were digested with BamHI and EcoRI (TaKaRa Bio, Shiga, Japan). The fused FP genes, mTurqoise2 (mTQ2), eGFP, Venus, mKOκ, and tdTomato (tdT), were amplified by PCR and digested with EcoRI and HindIII. All samples digested with a restriction enzyme were isolated via gel electrophoresis using a FastGene

Gel/PCR Extraction Kit (Nippon Genetics). Thereafter, the samples were mixed and cloned into the pRSETB vector (Invitrogen) using T4 ligase in Rapid Ligation Buffer (Promega). C-terminal–deleted mCRISPRed (mCRedΔC9) (*51*) and N-terminal–deleted Nluc (NlucΔN5) were fused in mCRedNL. C-terminal–deleted mCherry-XL (mCXLΔC7 or mCXLΔC2) (*52*) and NlucΔN5 were fused in mCXL7NL and mCXL2NL, and the constructs were named accordingly. These sequences were presented in the Supplementary Materials. Linkers in OeNL-r-mTQ2 and OeNL-r-eGFP were synthesized using primers. Sequences of NanoBiT system (Promega, LgBiT and SmBiT) in GPCR sensor were used in the original vector. They were replaced with the Nluc part of eNLEX by PCR. All plasmids were purified using the alkaline phosphatase method. The sequence was confirmed using dye terminator cycle sequencing with the BigDye Terminator v1.1 Cycle Sequencing kit (Thermo Fisher Scientific).

For the mammalian expression plasmids, cDNAs of eNLEX were amplified using the start codon. The fragments were then inserted into the pcDNA3 vector (Invitrogen) using BamHI and ApaI. For transfection into mammalian cells, the plasmids were purified using the PureYield Plasmid Miniprep System (Promega). The original eNL plasmids were used in a previous study (*6*) (CeNL: Addgene plasmid no. 85199, GeNL: Addgene plasmid no. 85200, YeNL: Addgene plasmid no. 85201, OeNL: Addgene plasmid no. 85202, and ReNL: Addgene plasmid no. 85203). A mammalian expression plasmid of Akaluc from RIKEN BRC (no. RDB15781) was used. A plasmid expressing Eluc was constructed based on pcDNA3, in which the original gene (Toyobo) was amplified and inserted using BamHI and EcoRI. ORCA-Y and CoxVIIIx2-ORCA-R [a duplicated mitochondrial targeting sequence derived from the subunit-VIII precursor of human cytochrome c oxidase (Cox-VIII) at the N terminus] were expressed by pcDNA3, which was used with BamHI and EcoRI to insert the gene described elsewhere (*35*). eNLEX members were targeted to the mitochondria, nucleus, and cell membrane by replacing the GeNL sequence in pcDNA3-CoxVIIIx2-GeNL, pcDNA3-GeNL-H2B [a DNA binding protein histone 2B (H2B) at the C terminus], and pcDNA3-Lyn-GeNL (a myristoylation and palmitoylation sequence from lyn kinase at the N terminus) described in the original paper (*6*) with GeNL-tdT, mCXL7NL, and OeNL-tdT sequences, respectively. Mammalian expression vectors for targeting ER (CeNL and GeNL), nucleolus (Nluc), lysosome (CeNL), and peroxisome (OeNL) were the same as those used in the original paper (*6*). The OeNL-mKOκ and ReNL-mKOκ lysosome targeting vectors were generated by replacing CeNL. For the expression of the GPCR sensor, the expression vector was constructed based on the preceding sensor (*44*).

For the expression of *Physcomitrella patens (P. patens)*, the pPGX6 vector from M. Hasebe (National Institute for Basic Biology) was used. The DNA sequences of eNLEX and actin 5′ region (*53*) were inserted in the vector.

Protein expression and purification

To express the eNLEX members with an N-terminal polyhistidine tag, the *E. coli* strain JM109[DE3] transformed with the expression vector was cultured at 23°C for 60 hours in LB bacterial growth medium supplemented with 0.1 mg ml^{-1} carbenicillin. The cultured cells were collected and disrupted by sonication (SONIFIER 150, BRANSON) after treatment with 40 μg ml^{-1} lysozyme. The recombinant proteins were purified from the supernatants using Ni-NTA agarose affinity columns (Qiagen). The protein concentration was measured using the Bradford method (protein assay kit, Bio-Rad) and adjusted by adding 20 mM Hepes buffer (pH 7.4).

Bioluminescent spectra measurement

The eNLEX spectra were measured using the photonic multichannel analyzer, PMA-12 (Hamamatsu Photonics), at room temperature with a 500-ms exposure. Coelenterazine-h (CTZh; Wako, final concentration, 5 μM) was used as the substrate. For confirmation of environmental effects (temperature and pH), purified eNLEX proteins (OeNL, OeNL-mTQ2, GeNL-tdT, and ReNL) were incubated in each condition for 1 min and the spectra were measured.

Detection of bioluminescence from *E. coli* using a smartphone camera

To capture the *E. coli* colonies via imaging, *E. coli* expressing each eNLEX member were colonized on an agar medium plate. Areas of each colony were coated by dropping 2% agarose solution containing 10 μM CTZh. Bioluminescence was detected using a camera on a smartphone (HUAWEI P40 Pro, dual-pixel sensor with 1220×10^4 pixels, F-number: 1.7). Images were captured in the dark at room temperature using a preset camera software in the Android OS (manual mode, ISO250, white balance: 6200 K, exposure time: 10 s, autofocus). To capture purified eNLEX via imaging, the proteins were diluted to 1 μM with 100 μl of dH_2O and dispended into a microtube. Twenty-five microliters of 50 μM CTZh in phosphate-buffered saline was subsequently added. The bioluminescence was captured in the dark at room temperature. Images were acquired using a preset camera software (manual mode, ISO250, white balance: 6200 K, exposure time: 0.5 s, autofocus).

Culture and transient transfection of mammalian cells

HeLa, HEK293, C2C12 (RIKEN BRC), and Neuro2A (from A. Takashima, Gakushuin University) were cultured in 24-well polystyrene flat-bottom dishes in Dulbecco's modified Eagle's medium (DMEM; Sigma) supplemented with 10% fetal bovine serum (FBS). The next day, the cells (50% confluency) were transfected with 0.5 μg $well^{-1}$ plasmid DNA using polyethyleneimine (PEI Max, Polysciences) and incubated for 16 hours at 37°C in 5% CO_2. The medium was changed, and the cells were cultured for an additional 24 hours.

Culture and transient transfection of *P. patens*

P. patens was provided by M. Sugita (Nagoya University). The protonemata was cultured at 25°C under continuous light on a solidified BCDATG medium. The expression vectors of eNLEX were introduced into protoplasts prepared from the protonemata by polyethylene glycol–mediated transformation. The protoplasts were incubated for 2 days and observed.

Preparation and bioluminescence imaging of cells

For microscopy, the transfected cells were recultured in collagen-coated 35-mm glass-bottom dishes for 16 hours. The medium was then replaced with phenol red–free DMEM/F12 containing 10% Hanks' balanced salt solution and 1% FBS. Furimazine (Promega) was used at a 500-fold dilution for the one-shot imaging of eNLs and time-lapse imaging of Ca^{2+}. For time-lapse imaging in Fig. 6, 1 mM Piv-FMZ substrate (*26*) was used at a 100-fold dilution. For time-lapse imaging in fig. S7A and movie S3, Endurazine (Promega) was used at a 100-fold dilution. For Akaluc and Eluc, 1 mM

Akalumine-HCl (Fujifilm-Wako) and 1 mM D-luciferin (Fujifilm-Wako) were added, respectively. For the HeLa cell spheroids, each transfected cell was cultured in a U-bottom multi-well dish for 1 day. The cells were collected, dispensed in the same wells, and cultured for 2 days in DMEM/F12 supplemented with 10% FBS. Furimazine was added at a 500-fold dilution immediately before observation. For the activation of GPCR, apelin-13 (Peptide Institute) for AG-TRL1, gastrin-1 (Peptide Institute) for CCKBR, endothelin-1 (Peptide Institute) for EDNRB, and somatostatin (Fujifilm-Wako) for SSTR2 were used. Bioluminescence was observed using IX-83 (Olympus) equipped with a color CMOS camera (ATR3CMOS-26000KPA, ToupTek, quantum efficiency peak: >80%). The condition was set using ImageView software (Bestscope) with a 7000 K white balance, 4 × 4 binning, and 10 to 50 times gain. The exposure time ranged from 15 to 30 s. Ca^{2+} imaging was performed for 5 s. For time-lapse cell imaging, images were captured at an exposure time of 1 min at 5-min intervals. The objective lenses (Olympus) were UPlanSApo 20× (one-shot images of a single cell), UPlanFL 10× (cell population and time-lapse images), PlanApo 60× (subcellular images), UPlanSApo 100× (calculation of the spatial resolution), and UPlanFL 4× (spheroid images). The observation condition was set at 37°C in 5% CO_2. For Ca^{2+} observation, cell stimulation was performed by dropping 20 μM histamine above the field of view. For fluorescence imaging, each FP in eNLEX was excited with a mercury lamp light and observed using the following filter cubes: U-FBNA (Olympus) for eGFP, U-FMCHE (Olympus) for tdTomato, and mCherry-XL.

The images were analyzed using the MetaMorph software (Molecular Devices). The noise in the image was reduced using an average filter in the software. The color separation in Fig. 6C was performed while converting the original RGB image to HSV using the Color Threshold program. The formula is presented in the Supplementary Materials. For the calculation of image resolution, Fourier ring correlation (FRC) (*54*) was used by a plugin of ImageJ. Line scattering was performed by the MetaMorph software.

Preparation and bioluminescence imaging of mouse

Transfected HEK293 cells were detached from the culture dish and injected under the skin of BALB/c Slc-nu/nu (15 to 16 g, 5 weeks, female) mice. Piv-FMZ (10 μM) in saline was also injected at the same site. The images were captured in the dark at room temperature using a smartphone camera and a preset camera software (manual mode, ISO5000, white balance: 6200 K, exposure time: 10 s, autofocus). Imaging involving the introduction of eNLEX proteins was performed using the same species of mice. Purified protein (100 μg) was introduced intravenously and allowed to circulate for 10 min. Additionally, 10 μl of furimazine was administrated intravenously. The images were captured using a color CMOS camera (MAX62-AC, ToupTek). Animal experiments were approved by the Institutional Animal Care and Use Committee of their institution.

Supplementary Materials

The PDF file includes:

Supplementary Text
Figs. S1 to S19
Legends for movies S1 to S5

Other Supplementary Material for this manuscript includes the following:

Movies S1 to S5

REFERENCES AND NOTES

1. T. Ichimura, T. Kakizuka, K. Horikawa, K. Seiriki, A. Kasai, H. Hashimoto, K. Fujita, T. M. Watanabe, T. Nagai, Exploring rare cellular activity in more than one million cells by a transscale scope. *Sci. Rep.* **11**, 16539 (2021).
2. J. Livet, T. A. Weissman, H. Kang, R. W. Draft, J. Lu, R. A. Bennis, J. R. Sanes, J. W. Lichtman, Transgenic strategies for combinatorial expression of fluorescent proteins in the nervous system. *Nature* **450**, 56–62 (2007).
3. M. N. Leiwe, S. Fujimoto, T. Baba, D. Moriyasu, B. Saha, R. Sakaguchi, S. Inagaki, T. Imai, Automated neuronal reconstruction with super-multicolour Tetbow labelling and threshold-based clustering of colour hues. *Nat. Commun.* **15**, 5279 (2024).
4. T. F. Massoud, S. S. Gambhir, Molecular imaging in living subjects: Seeing fundamental biological processes in a new light. *Genes Dev.* **17**, 545–580 (2003).
5. A. M. Loening, A. M. Wu, S. S. Gambhir, Red-shifted Renilla reniformis luciferase variants for imaging in living subjects. *Nat. Methods* **4**, 641–643 (2007).
6. S. Iwano, M. Sugiyama, H. Hama, A. Watakabe, N. Hasegawa, T. Kuchimaru, K. Z. Tanaka, M. Takahashi, Y. Ishida, J. Hata, S. Shimozono, K. Namiki, T. Fukano, M. Kiyama, H. Okano, S. Kizaka-Kondoh, T. J. McHugh, T. Yamamori, H. Hioki, S. Maki, A. Miyawaki, Single-cell bioluminescence imaging of deep tissue in freely moving animals. *Science* **359**, 935–939 (2018).
7. Y. Su, J. R. Walker, Y. Park, T. P. Smith, L. X. Liu, M. P. Hall, L. Labanieh, R. Hurst, D. C. Wang, L. P. Encell, N. Kim, F. Zhang, M. A. Kay, K. M. Casey, R. G. Majzner, J. R. Cochran, C. L. Mackall, T. A. Kirkland, M. Z. Lin, An optimized bioluminescent substrate for non-invasive imaging in the brain. *Nat. Chem. Biol.* **19**, 731–739 (2023).
8. V. R. Viviani, E. J. H. Bechara, Y. Ohmiya, Cloning, sequence analysis, and expression of active phrixothrix railroad-worms luciferases: Relationship between bioluminescence spectra and primary structures. *Biochemistry* **38**, 8271–8279 (1999).
9. V. R. Viviani, A. C. R. Silva, G. L. O. Perez, R. V. Santelli, E. J. H. Bechara, F. C. Reinach, Cloning and molecular characterization of the cDNA for the Brazilian larval Click-beetle Pyrearinus termitilluminans luciferase. *Photochem. Photobiol.* **70**, 254–260 (1999).
10. K. Suzuki, T. Kimura, H. Shinoda, G. Bai, M. J. Daniels, Y. Arai, M. Nakano, T. Nagai, Five colour variants of bright luminescent protein for real-time multicolour bioimaging. *Nat. Commun.* **7**, 13718 (2016).
11. M. P. Hall, J. Unch, B. F. Binkowski, M. P. Valley, B. L. Butler, M. G. Wood, P. Otto, K. Zimmerman, G. Vidugiris, T. Machleidt, M. B. Robers, H. A. Benink, C. T. Eggers, M. R. Slater, P. L. Meisenheimer, D. H. Klaubert, F. Fan, L. P. Encell, K. V. Wood, Engineered luciferase reporter from a deep sea shrimp utilizing a novel imidazopyrazinone substrate. *ACS Chem. Biol.* **7**, 1848–1857 (2012).
12. H. Tsurui, H. Nishimura, S. Hattori, S. Hirose, K. Okumura, T. Shirai, Seven-color fluorescence imaging of tissue samples based on Fourier spectroscopy and singular value decomposition. J. Histochem. Cytochem. **48**, 653–662 (2000).
13. A. S. Dixon, M. K. Schwinn, M. P. Hall, K. Zimmerman, P. Otto, T. H. Lubben, B. L. Butler, B. F. Binkowski, T. Machleidt, T. A. Kirkland, M. G. Wood, C. T. Eggers, L. P. Encell, K. V. Wood, NanoLuc complementation reporter optimized for accurate measurement of protein interactions in cells. *ACS Chem. Biol.* **11**, 400–408 (2016).
14. T. Zimmermann, J. Rietdorf, R. Pepperkok, Spectral imaging and its applications in live cell microscopy. *FEBS Lett.* **546**, 87–92 (2003).
15. J. Seo, Y. Sim, J. Kim, H. Kim, I. Cho, H. Nam, Y. G. Yoon, J. B. Chang, PICASSO allows ultra-multiplexed fluorescence imaging of spatially overlapping proteins without reference spectra measurements. *Nat. Commun.* **13**, 2475 (2022).
16. A. M. Valm, S. Cohen, W. R. Legant, J. Melunis, U. Hershberg, E. Wait, A. R. Cohen, M. W. Davidson, E. Betzig, J. Lippincott-Schwartz, Applying systems-level spectral imaging and analysis to reveal the organelle interactome. *Nature* **546**, 162–167 (2017).
17. M. A. J. Gorris, A. Halilovic, K. Rabold, A. van Duffelen, I. N. Wickramasinghe, D. Verweij, I. M. N. Wortel, J. C. Textor, I. J. M. de Vries, C. G. Figdor, Eight-color multiplex immunohistochemistry for simultaneous detection of multiple immune checkpoint molecules within the tumor microenvironment. *J. Immunol.* **200**, 347–354 (2018).
18. K. Chen, R. Yan, L. Xiang, K. Xu, Excitation spectral microscopy for highly multiplexed fluorescence imaging and quantitative biosensing. *Light Sci. Appl.* **10**, 97 (2021).
19. J. Yang, D. Cumberbatch, S. Centanni, S. Q. Shi, D. Winder, D. Webb, C. H. Johnson, Coupling optogenetic stimulation with NanoLuc-based luminescence (BRET) Ca^{++} sensing. *Nat. Commun.* **7**, 13268 (2016).
20. S. Inagaki, H. Tsutsui, K. Suzuki, M. Agetsuma, Y. Arai, Y. Jinno, G. Bai, M. J. Daniels, Y. Okamura, T. Matsuda, T. Nagai, Genetically encoded bioluminescent voltage indicator for multi-purpose use in wide range of bioimaging. *Sci. Rep.* **7**, 42398 (2017).
21. L. F. Morales-Curiel, A. C. Gonzalez, G. Castro-Olvera, L. L. Lin, M. El-Quessny, M. Porta-de-la-Riva, J. Severino, L. B. Morera, V. Venturini, V. Ruprecht, D. Ramallo, P. Loza-Alvarez, M. Krieg, Volumetric imaging of fast cellular dynamics with deep learning enhanced bioluminescence microscopy. *Commun. Biol.* **5**, 1330 (2022).
22. Z. Yao, C. K. Brennan, L. Scipioni, H. Chen, K. K. Ng, G. Tedeschi, K. Parag-Sharma, A. L. Amelio, E. Gratton, M. A. Digman, J. A. Prescher, Multiplexed bioluminescence microscopy via phasor analysis. *Nat. Methods* **19**, 893–898 (2022).

23. R. Arts, I. den Hartog, S. E. Zijlema, V. Thijssen, S. H. van der Beelen, M. Merkx, Detection of antibodies in blood plasma using bioluminescent sensor proteins and a smartphone. *Anal. Chem.* **88**, 4525–4532 (2016).
24. M. Hattori, S. Shirane, T. Matsuda, K. Nagayama, T. Nagai, Smartphone-based portable bioluminescence imaging system enabling observation at various scales from whole mouse body to organelle. *Sensors* **20**, 7166 (2020).
25. K. Tomimuro, K. Tenda, Y. Ni, Y. Hiruta, M. Merkx, D. Citterio, Thread-based bioluminescent sensor for detecting multiple antibodies in a single drop of whole blood. *ACS Sens.* **5**, 1786–1794 (2020).
26. Y. Nakajima, T. Yamazaki, S. Nishii, T. Noguchi, H. Hoshino, K. Niwa, V. R. Viviani, Y. Ohmiya, Enhanced beetle luciferase for high-resolution bioluminescence imaging. *PLOS ONE* **5**, e10011 (2010).
27. Y. Mizui, M. Eguchi, M. Tanaka, Y. Ikeda, H. Yoshimura, T. Ozawa, D. Citterio, Y. Hiruta, Long-term single cell bioluminescence imaging with C-3 position protected coelenterazine analogues. *Org. Biomol. Chem.* **19**, 579–586 (2020).
28. K. M. Riching, S. Mahan, C. R. Corona, M. McDougall, J. D. Vasta, M. B. Robers, M. Urh, D. L. Daniels, Quantitative live-cell kinetic degradation and mechanistic profiling of PROTAC mode of action. *ACS Chem. Biol.* **13**, 2758–2770 (2018).
29. M. Orioka, M. Eguchi, Y. Mizui, Y. Ikeda, A. Sakama, Q. Li, H. Yoshimura, T. Ozawa, D. Citterio, Y. Hiruta, A series of furimazine derivatives for sustained live-cell bioluminescence imaging and application to the monitoring of myogenesis at the single-cell level. *Bioconjug. Chem.* **33**, 496–504 (2022).
30. A. Sakama, M. Orioka, Y. Hiruta, Current advances in the development of bioluminescent probes toward spatiotemporal trans-scale imaging. *Biophys. Physicobiol.* **21**, e21004 (2024).
31. W. Burger, M. J. Burge, *Digital Image Processing: An Algorithmic Introduction Using Java* (Springer, 2008).
32. E. J. Aird, K. J. Tompkins, M. P. Ramirez, W. R. Gordon, Enhanced molecular tension sensor based on bioluminescence resonance energy transfer (BRET). *ACS Sens.* **5**, 34–39 (2020).
33. Y. Itoh, M. Hattori, T. Wazawa, Y. Arai, T. Nagai, Ratiometric bioluminescent indicator for simple and rapid diagnosis of bilirubin. *ACS Sens.* **6**, 889–895 (2021).
34. M. Hattori, N. Sugiura, T. Wazawa, T. Matsuda, T. Nagai, Ratiometric bioluminescent indicator for a simple and rapid measurement of thrombin activity using a smartphone. *Anal. Chem.* **93**, 13520–13526 (2021).
35. M. Hattori, T. Matsuda, T. Nagai, Method for detecting emission spectral change of bioluminescent ratiometric indicators by a smartphone. *Methods Mol. Biol.* **2274**, 295–304 (2021).
36. T. Nakatsu, S. Ichiyama, J. Hiratake, A. Saldanha, N. Kobashi, K. Sakata, H. Kato, Structural basis for the spectral difference in luciferase bioluminescence. *Nature* **440**, 372–376 (2006).
37. T. Kuchimaru, S. Iwano, M. Kiyama, S. Mitsumata, T. Kadonosono, H. Niwa, S. Maki, S. Kizaka-Kondoh, A luciferin analogue generating near-infrared bioluminescence achieves highly sensitive deep-tissue imaging. *Nat. Commun.* **7**, 11856 (2016).
38. H. W. Yeh, O. Karmach, A. Ji, D. Carter, M. M. Martins-Green, H. W. Ai, Red-shifted luciferase-luciferin pairs for enhanced bioluminescence imaging. *Nat. Methods* **14**, 971–974 (2017).
39. K. Saito, Y. F. Chang, K. Horikawa, N. Hatsugai, Y. Higuchi, M. Hashida, Y. Yoshida, T. Matsuda, Y. Arai, T. Nagai, Luminescent proteins for high-speed single-cell and whole-body imaging. *Nat. Commun.* **3**, 1262 (2012).
40. A. Takai, M. Nakano, K. Saito, R. Haruno, T. M. Watanabe, T. Ohyanagi, T. Jin, Y. Okada, T. Nagai, Expanded palette of Nano-lanterns for real-time multicolor luminescence imaging. *Proc. Natl. Acad. Sci. U.S.A.* **112**, 4352–4356 (2015).
41. F. X. Schaub, M. S. Reza, C. A. Flaveny, W. Li, A. M. Musicant, S. Hoxha, M. Guo, J. L. Cleveland, A. L. Amelio, Fluorophore-Nanoluc BRET reporters enable sensitive in vivo optical imaging and flow cytometry for monitoring tumorigenesis. *Cancer Res.* **75**, 5023–5033 (2015).
42. J. Chu, Y. Oh, A. Sens, N. Ataie, H. Dana, J. J. Macklin, T. Laviv, E. S. Welf, K. M. Dean, F. Zhang, B. B. Kim, C. T. Tang, M. Hu, M. A. Baird, M. W. Davidson, M. A. Kay, R. Fiolka, R. Yasuda, D. S. Kim, H. L. Ng, M. Z. Lin, A bright cyan-excitable orange fluorescent protein facilitates dual-emission microscopy and enhances bioluminescence imaging in vivo. *Nat. Biotechnol.* **34**, 760–767 (2016).
43. E. Goyet, N. Bouquier, V. Ollendorff, J. Perroy, Fast and high resolution single-cell BRET imaging. *Sci. Rep.* **6**, 28231 (2016).
44. N. Misawa, A. K. M. Kafi, M. Hattori, K. Miura, T. Ozawa, Rapid and high-sensitivity cell-based assays of protein-protein interactions using split click beetle luciferase complementation: An approach to the study of G-protein-coupled receptors. *Anal. Chem.* **82**, 2552–2560 (2010).
45. H. Kim, I. Y. Baek, J. Seong, Genetically encoded fluorescent biosensors for GPCR research. *Front. Cell Dev. Biol.* **10**, 1007893 (2022).
46. B. Vladan, S. Oliver, Smartphone imaging technology and its applications. *Adv. Opt. Tech.* **10**, 145–232 (2021).
47. A. Isomura, F. Ogushi, H. Kori, R. Kageyama, Optogenetic perturbation and bioluminescence imaging to analyze cell-to-cell transfer of oscillatory information. *Genes Dev.* **31**, 524–535 (2017).
48. N. Komatsu, K. Terai, A. Imanishi, Y. Kamioka, K. Sumiyama, T. Jin, Y. Okada, T. Nagai, M. Matsuda, A platform of BRET-FRET hybrid biosensors for optogenetics, chemical screening, and in vivo imaging. *Sci. Rep.* **8**, 8984 (2018).
49. A. A. Kotlobay, K. S. Sarkisyan, Y. A. Mokrushina, M. Marcet-Houben, E. O. Serebrovskaya, N. M. Markina, L. Gonzalez Somermeyer, A. Y. Gorokhovatsky, A. Vvedensky, K. V. Purtov, V. N. Petushkov, N. S. Rodionova, T. V. Chepurnyh, L. I. Fakhranurova, E. B. Guglya, R. Ziganshin, A. S. Tsarkova, Z. M. Kaskova, V. Shender, M. Abakumov, T. O. Abakumova, I. S. Povolotskaya, F. M. Eroshkin, A. G. Zaraisky, A. S. Mishin, S. V. Dolgov, T. Y. Mitiouchkina, E. P. Kopantzev, H. E. Waldenmaier, A. G. Oliveira, Y. Oba, E. Barsova, E. A. Bogdanova, T. Gabaldon, C. V. Stevani, S. Lukyanov, I. V. Smirnov, J. I. Gitelson, F. A. Kondrashov, I. V. Yampolsky, Genetically encodable bioluminescent system from fungi. *Proc. Natl. Acad. Sci. U.S.A.* **115**, 12728–12732 (2018).
50. C. Gregor, J. K. Pape, K. C. Gwosch, T. Gilat, S. J. Sahl, S. W. Hell, Autonomous bioluminescence imaging of single mammalian cells with the bacterial bioluminescence system. *Proc. Natl. Acad. Sci. U.S.A.* **116**, 26491–26496 (2019).
51. M. Erdogan, A. Fabritius, J. Basquin, O. Griesbeck, Targeted in situ protein diversification and intra-organelle validation in mammalian cells. *Cell Chem. Biol.* **27**, 610–621.e5 (2020).
52. M. Srijit, M. Premashis, H. Sheng-Ting, V. Felix, F. Pia, E. P. Amy, J. Ralph, Directed evolution of a bright variant of mCherry: Suppression of nonradiative decay by fluorescence lifetime selections. *J. Phys. Chem. B* **126**, 4659–4668 (2022).
53. A. Weise, M. Rodriguez-Franco, B. Timm, M. Hermann, S. Link, W. Jost, G. Gorr, Use of Physcomitrella patens actin 5′ regions for high transgene expression: Importance of 5′ introns. *Appl. Microbiol. Biotechnol.* **70**, 337–345 (2006).
54. R. P. Nieuwenhuizen, K. A. Lidke, M. Bates, D. L. Puig, D. Grunwald, S. Stallinga, B. Rieger, Measuring image resolution in optical nanoscopy. *Nat. Methods* **10**, 557–562 (2013).

Acknowledgments: We thank T. Ozawa, M. Hasebe, M. Sugita, and A. Takashima for providing us with research materials. **Funding:** This study was partially supported by grants from the JST CREST Program (no. JPMJCR20H9 to T.N.); Ministry of Education, Culture, Sports, Science, and Technology (MEXT) (no. 18H05410 to T.N. and no. 21H00437 to Y.H.); New Energy and Industrial Technology Development Organization (no. 22681865 to T.N.); and the Japan Society for the Promotion of Science (JSPS) (no. 22 K05153 to M.H.). **Author contributions:** Conceptualization: M.H. and T.N. Methodology: M.H., T.W., M.O., and Y.H. Investigation: M.H. Supervision: T.N. Writing—original draft: M.H. Writing—review and editing: T.W., M.O., Y.H., and T.N. **Competing interests:** The authors declare that they have no competing interests. **Data and materials availability:** All data needed to evaluate the conclusions in the paper are present in the paper and/or the Supplementary Materials. The expression vector for *P. patens* can be provided by the National Institute for Basic Biology pending scientific review and a completed material transfer agreement. Requests for the vector should be submitted to M. Hasebe.

Submitted 27 March 2024
Accepted 18 December 2024
Published 22 January 2025
10.1126/sciadv.adp4750